# 4 Outer Detector

## 4.1 Introduction

In this chapter, we describe the performance and design of the outer detector system for LZ. The principal signal we seek, that of a WIMP scatter depositing 5 $\mathrm{keV_{nr}}$ to 50 $\mathrm{keV_{nr}}$ of energy in the central 5.6 t volume of LXe, will never be accompanied by deposited energy in the surrounding detector components. In contrast, many dominant backgrounds that might fake a WIMP signal will deposit energy not only in the central Xe detector but also in the material surrounding it. If we are able to detect these secondary interactions, we can veto the background event. Table 1.6.1 shows the major backgrounds in LZ, which include signals from gammas with energies in the few-MeV range and neutrons from ($\alpha$,n) reactions or created by cosmic-ray interactions.

To reduce these backgrounds, we surround the large active Xe volume with an integrated detector capable of tagging gamma rays and neutrons with high efficiency. Three detector elements are used to achieve this performance:

- The instrumented "skin" of the Xe, the region outside the LXe TPC,
- The gadolinium-loaded liquid scintillator (Gd-LS), and
- The portion of the surrounding water that is instrumented as a muon veto.

The outer detector system comprises the scintillator and water systems. In addition to the performance of the integrated veto system, this chapter describes the design of the outer detector system and modifications needed in the water tank to accommodate the LZ experiment.

## 4.2 Function and Performance

The outer detector serves two critical functions:

1. **To veto neutron and gamma backgrounds with high efficiency.** Although the outer region of the LXe shields the inner region very efficiently, the outer half of the Xe could not be used as part of the fiducial mass without an external veto. By instrumenting the outer skin of the LXe and adding the outer liquid scintillator detector, we are able to nearly double the fraction of the Xe in which very-low backgrounds are achievable. The outer liquid scintillator detector is essential for vetoing neutrons, the background that most closely mimics dark-matter scattering.

   One risk to the performance of the LZ detector is that some material very close to the LXe could have a concentration of radioactive impurities higher than expected. The combination of the LXe skin and the outer detector serves to mitigate this risk. The integrated veto can suppress most backgrounds even if they are significantly higher than the design goals, with only a slight reduction in fiducial volume.

2. **To help characterize and measure the background.** A claim of a WIMP signal would require extraordinary supporting evidence. The outer detector will provide crucial supporting evidence necessary to establish a discovery. In particular, the NR background to a WIMP signal can be estimated by measuring the number of low-energy deposit scatters in the TPC which are followed by neutron captures in the outer detector.

The major non-neutrino background sources in LZ are neutrons and gammas from components within the cryostat and beta decays from radon and krypton distributed throughout the Xe. The principal goal of the integrated veto system is to reduce the effect of neutron and gamma backgrounds to a level smaller than that caused by radon and krypton over a very large fraction of the active LXe.

Neutrons represent a particularly troublesome background in the absence of an external veto. A neutron scatter produces a nuclear recoil (NR), as does a WIMP scatter, and after scattering they can escape the TPC and skin more easily than a gamma. The neutron background, which is principally produced in ($\alpha$,n) reactions in materials near the LXe, is more difficult to predict than the gamma background. If a possible WIMP signal is seen, the outer detector will contribute to the identification and estimation of the neutron background.

The design requirement for NR background is stringent (see Chapter 9). Without the outer detector, the neutron background would exceed our requirements, so meeting the sensitivity target requires a veto efficiency of greater than 90 % for neutrons escaping the TPC.

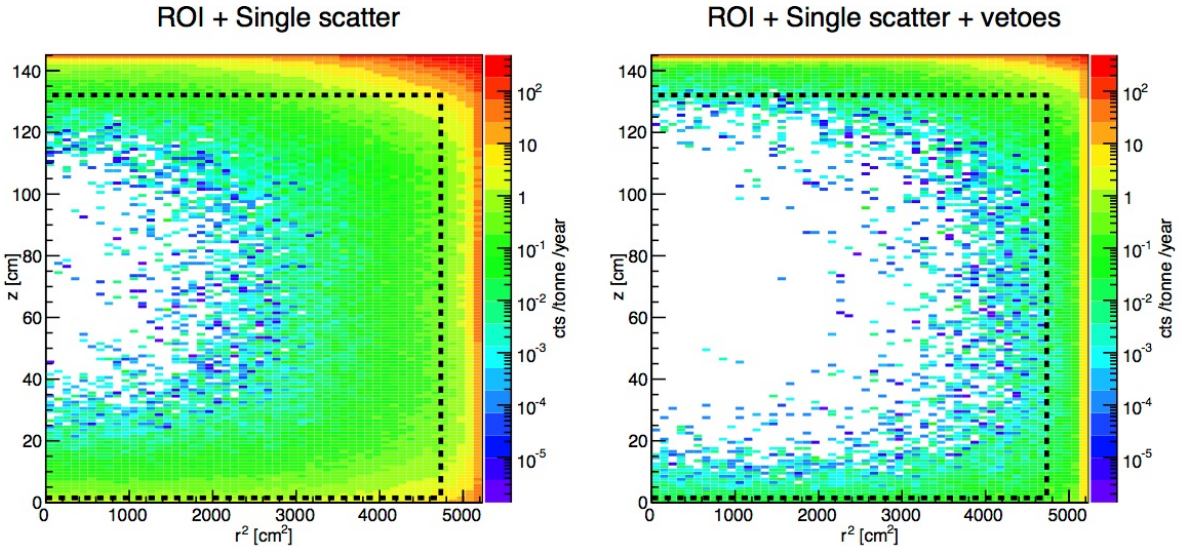


**Figure 4.2.1:** Total NR background plus ER leakage from material radioactivity for sources external to the LXe in the TPC, counted over a 6 keV to 30 keV acceptance region; a discrimination efficiency of 99.5 % is applied to ERs from beta decays and gamma rays. Left: Single scatters only, no vetoing by the anti-coincidence systems. Right: Adding the combination of both the skin veto and the outer detector. The dashed line shows the boundary of the 5.6 tonnes fiducial mass.

The principal sources of gamma background are components in direct contact with the LXe volume, such as the PMTs, the PTFE reflectors, and the titanium inner vessel. Gammas in the few-MeV range can scatter at small angles in the outer region of the TPC, depositing 0.5 keV to 6.5 keV of energy corresponding to the WIMP signal region, and then exit the TPC without a second scatter. Meeting our requirement (see Chapter 12) requires a veto efficiency of >70 % for such gammas.

We have carried out simulations to characterize the impact of the outer detector on the background characteristics of the detector. The results of these simulations are captured in Figure 4.2.1, which shows the spatial distribution of the neutron backgrounds that scatter only once in the LXe volume.

The left panel of Figure 4.2.1 shows the distribution of single scatters from backgrounds originating from fixed contamination, such as uranium and thorium, which generate neutrons that scatter in the Xe TPC, as well as gamma rays which produce ERs that leak into the NR band. The figures plot depth ($z$) versus radius-squared, so that the area on the plot is proportional to the volume of LXe. The central region is, as expected,

extraordinarily free of background. But the neutron background is much higher within ≈20 cm of the outer structures. The dashed black line indicates the 5.6 t fiducial volume. Without using information from the LXe skin or the outer detector, the fiducial mass is a bit less than half of the active LXe. Most of the active LXe itself in this case is used as a veto rather than as target material for WIMPs. If one of the component materials in the cryostat were to have a larger amount of radioactivity than the design target, even less of the active LXe would be in the fiducial volume.

The right panel of Figure 4.2.1 shows the performance when vetoing events that also deposit energy in either the instrumented LXe skin or the outer detector. The dashed line shows that the fiducial volume can be extended to within a few centimeters of the edge of the active LXe. The integrated veto system enables a fiducial volume of 5.6 t, almost twice as large as for a stand-alone LXe TPC. Even if the neutron backgrounds were significantly higher than assumed in this study, the very-low background needed for effective operation of LZ could be maintained by reducing the 5.6 t fiducial volume by only a very small amount.

Because of the large surface area of the LXe vessel, the fiducial volume increases by about 270 kg for every additional centimeter thickness of LXe at the boundary. To meet the LZ background requirements for >5.6 t fiducial volume without using an external veto would require a TPC containing 11 t, 4 t more than the LZ design value.

## 4.3 Outer Detector Overview

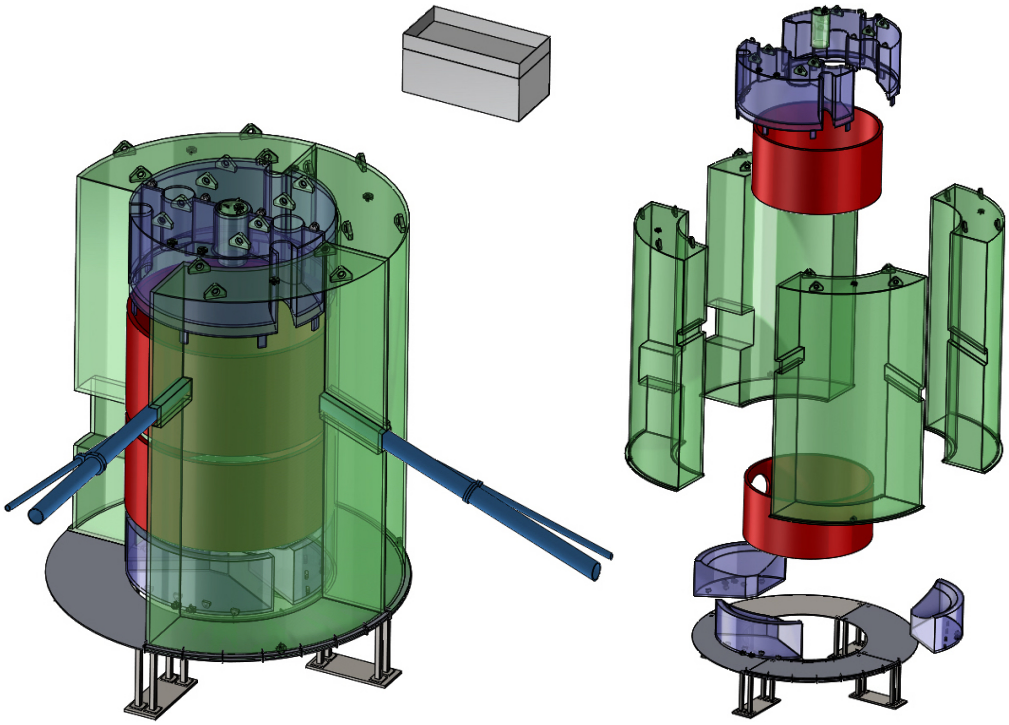

**Figure 4.3.1:** Layout of the LZ outer detector system, assembled on the left, and exploded to display the ten acrylic tanks, water displacers (in red), and stand, on the right. The tanks will be filled with Gd-LS, and the largest are the four quarter-tanks on the sides. Two tanks cover the top, and three the bottom. A small cylindrical vessel fits into a cutout at the center of the top tanks, replacing a YBe source for most running. The grey box is a reservoir for liquid scintillator.

The proposed layout of the LZ outer detector is shown in Figure 4.3.1. A hermetic detector is built from ten vessels fabricated from UVT acrylic. The use of segmented vessels allows fabrication to take place at the manufacturer's facility at considerable cost savings. The sizes of the vessels are chosen to allow straightforward insertion into the water tank and assembly of the full detector inside the water tank. Structural finite element analyses (FEAs) of the vessels have been performed to validate the design without introducing more inert material than is needed for safe operation. The acrylic for the side vessels is 1 inch thick; for the top and bottom vessels, the acrylic is 0.5 inch thick except for the top wall of the top vessel and the bottom wall of the bottom vessel.

The vessels will be viewed by 120 8 inch Hamamatsu R5912 PMTs. The PMTs are mounted on stainless steel frames in the water tank, separated from the Gd-LS vessels by 84 cm of ultrapure water. This arrangement gives a light-collection efficiency of about 7 % averaged over the volume of the outer detector, corresponding to a light yield of about 130 photo-electrons for a 1 MeV energy deposit. The water shields the Gd-LS from gammas that originate in the R5912 tubes. A low-density water displacer will be used to fill in the gaps between the cryostat and the acrylic vessels and the gaps around the penetrations, to reduce the probability of absorption in water. White diffuse reflector will be placed on all available surfaces to improve collection of the scintillation light.

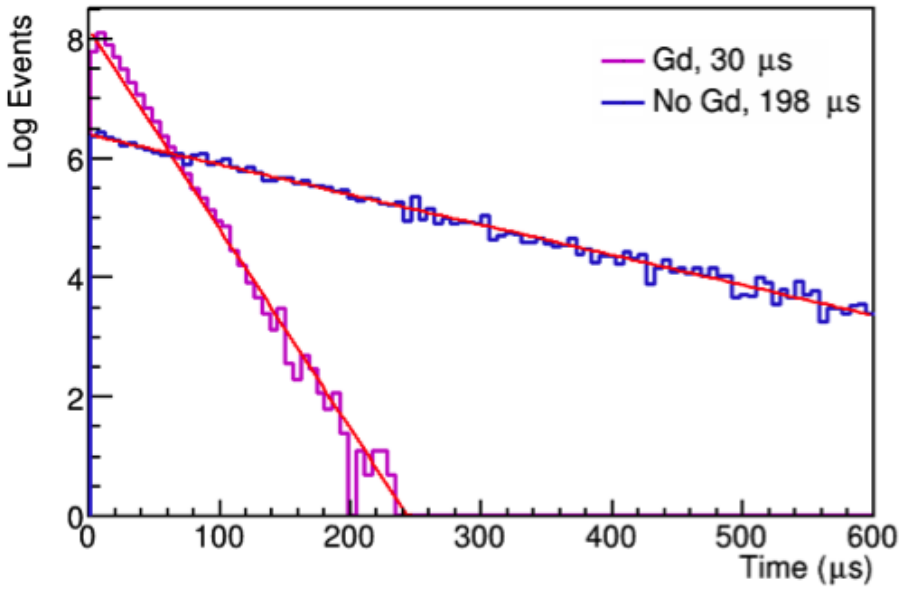


**Figure 4.3.2:** The simulated distribution of capture times for thermal neutrons in the outer detector for liquid scintillator with and without 0.1 % Gd.

Simulation of the veto performance showed that the veto efficiency varies slowly with the thickness of the scintillator in the outer detector over the range 50 to 80 cm. This thickness is therefore chosen to reduce the risk of problems during fabrication and assembly. To insert the side vessels into the water tank easily, the scintillator thickness needs to be no greater than 70 cm. Cleaning the side vessels during fabrication requires that the thickness be no less than 61 cm, which fixed the side tank scintillator thickness.

The radioactivity in the mine walls causes a flux of gamma rays to impinge on the water tank. The thinnest portions of water are at the top and bottom of the tank. The top and bottom tanks, as well as the vertical extent of the side tanks, were adjusted to reduce the rate caused by penetrating gamma rays at the top and bottom, without significant loss in neutron veto efficiency. Our simulation indicates a surviving rate of order

100 Hz, however, simulation of the tiny fraction of surviving penetrating gammas is challenging. The "LS screener" campaign in late 2016, described briefly in Section 4.5, will move a small LS detector through a variety of vertical positions in the water, to test the simulation.

The liquid scintillator is based upon a linear-alkylbenzene (LAB) solvent, which is a hydrocarbon chain with one benzene ring attached. LAB has a flashpoint that exceeds that of diesel fuel, and the safety aspects of diesel fuel in an underground facility have been explored and defined. The LAB is loaded with Gd, 0.1 % by mass, via an organic chelating agent, trimethyl hexanoic acid (TMHA). This scintillator mix with 0.1 % Gd doping was used by Chooz [1], Palo Verde [2], and Daya Bay [3]. The specific approach adopted by LZ is very similar to that used in the Daya Bay neutrino experiment, but with additional purification to achieve a lower radioactivity levels from uranium/thorium/potassium (U/Th/K) impurities.

Gadolinium is added to the scintillator to increase the efficiency for tagging neutrons while maintaining low veto deadtime. The benefit of using Gd and scintillator for this purpose was demonstrated in the ZEPLIN series of experiments. About 90 % of the neutrons which moderate to thermal energies in the scintillator are captured on $^{157}$Gd or $^{155}$Gd, releasing 3-4 gammas with total energy of 7.9 MeV ($^{157}$Gd) or 8.5 MeV ($^{155}$Gd); the remaining 10 % of these neutrons are captured on hydrogen, producing a single 2.2 MeV gamma. The Gd captures are tagged with higher efficiency because of the multiple gammas produced and the high energy of those gammas. The Gd capture also reduces the neutron capture time to about 30 µs, compared with about 200 µs in scintillator without Gd. Figure 4.3.2 shows the simulated capture time for low-energy neutrons entering the outer detector. The fast capture helps reduce deadtime for the veto system.

A veto window of 125 µs after a WIMP candidate is matched to the capture time with Gd. However, our detailed simulations have shown that 5 % to 10 % of neutrons actually capture in the acrylic, and can be accomodated by a longer veto window. Our goal is to use a veto window of 500 µs, which we use in our simulation studies. To maintain a deadtime <5 % for a veto window 500 µs, we must achieve our goal of a total OD rate below 100 Hz. We can simultaneously achieve an inefficiency <5 % and deadtime <5 % with if the OD rate is 300 Hz, and we reduce our veto window to 170 µs.

## 4.4 Mechanical Systems

### 4.4.1 Acrylic Vessels

The 17.2 t of scintillator liquid are contained in nine permanent acrylic vessels, as shown in Figure 4.3.1: four tall vessels on the sides, two vessels that form a plug on the top, and three vessels that form a plug at the bottom. A small tenth vessel is used when the YBe calibration source is not in use. Taken together, the LS system forms a ≈61 cm thickness of Gd-LS surrounding the LXe vessel, with several penetrations for connections to the Xe detector and for calibration systems. Similar acrylic vessels were used for the Daya Bay Antineutrino Detectors [3].

The masses and volumes of the ten vessels are shown in Table 4.4.1. The side vessels represent the largest part of the veto mass, holding about 89 % of the scintillator. Each of the four side vessels is 375 cm high, extends in radius from 97.5 to 163.5 cm, and covers one-quarter of the full azimuth. A vessel is supported and anchored to a stainless steel base frame, which is in turn anchored to a base plate installed on the floor of the water tank. The net upward force on each side vessel when filled is 4,940 N.

**Table 4.4.1:** The volume and masses of the scintillator vessels

| | Acrylic Mass kg | LS Volume $m^3$ | LS Mass kg | Net buoyant force N |
|---|---|---|---|---|
| **YBe source plug (1)** | 8 | 0.025 | 22 | 21 |
| **Side Tank (4)** | 684 | 4.431 | 3,823 | 4,940 |
| **Top Tank (2)** | 116 | 0.648 | 559 | 699 |
| **Bottom Tank (3)** | 59 | 0.313 | 270 | 333 |
| **TOTAL** | 3,154 | 19.984 | 17,242 | 22,178 |

The two top vessels and the YBe plug form cylinder that fits inside the side vessels. At the thinnest point, the top(bottom) LS thickness is 40 cm(34.5 cm)-thick, and at the thickest, the top(bottom) LS thickness is 62 cm(57 cm)-thick. These tanks will be anchored from the top of the outer cryostat vessel. The three bottom vessels form a cylinder of the similar thickness at the bottom. The penetrations for services and calibrations are positioned within the gaps between the acrylic vessel and in cutouts in the acrylic vessels.

Filling the acrylic vessel with LS and the water tank with water at the same time makes it possible to engineer the vessels with acrylic 1 inch thick, much thinner than the 4 inch thickness that would be required if the vessels were ever filled with LS and just air surrounding them. The level of scintillator in each side tank will be kept near the optimum level for minimum stress, about 10 inch above the height of water in the tank. Figure 4.4.1 shows the results of a finite element analysis of the stress on the side vessels during the filling process. During filling the stresses will be kept below 1,000 psi, well below the short-term maximum stress of 3,000 psi. Once the final state has been reached, the maximum stress is 153 psi, well below the long-term crazing limit of 700 psi. The maximum deformation at that stage will be 0.05 inch.

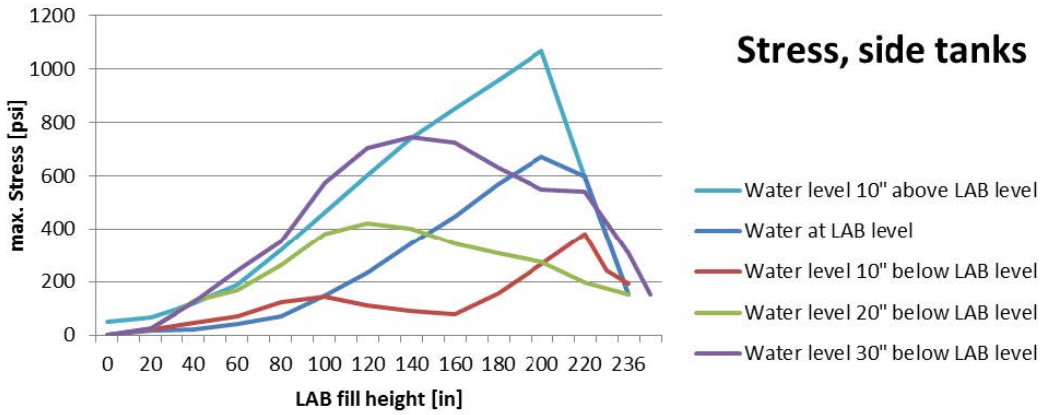


**Figure 4.4.1:** Stress on the side scintillator tanks during filling, from a finite element analysis. The scintillator height in each vessel will be maintained within the range shown in these five plots. The maximum stress will be maintained well below the short term maximum stress of 3,000 psi.

The flanges on the detector cryostat protrude about 2 inch outside the cylindrical surface. To avoid building recesses in the acrylic vessels to accommodate these protrusions, a low-density closed-cell foam will be

installed as a water displacer around the outer vessel of the cryostat. This maintains low absorption of gammas between the scintillator and the LXe skin detector.

The vessels will be cleaned inside and leak-checked at the fabrication vendor. They will be wrapped in protective sheets at that time, and placed in double bags before being crated for shipping. The protective sheets will be removed after they are installed in the water tank. The final cleaning of the outside of the vessel will be done at that time.

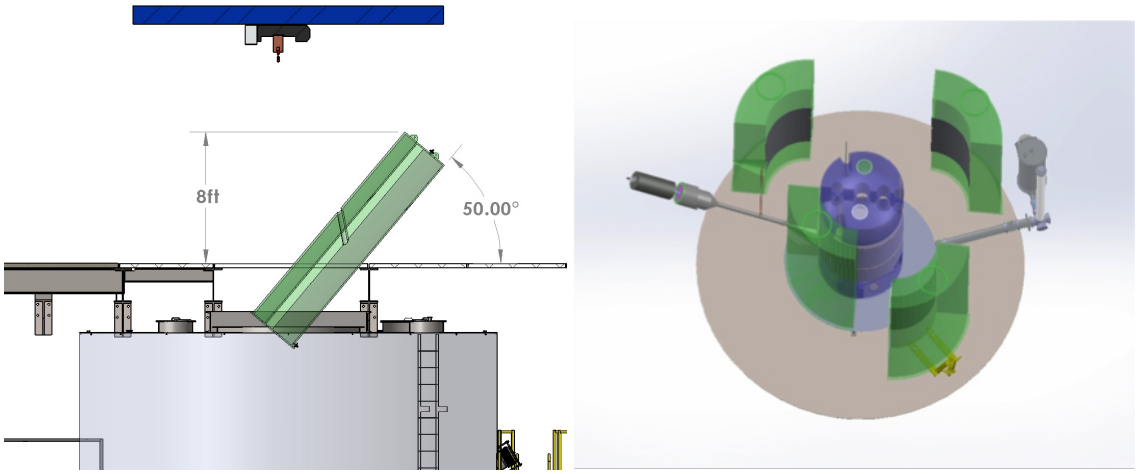


**Figure 4.4.2:** Two steps in the assembly sequence. The figure on the left shows one of the quadrant vessels at the point of maximum height above the water tank. The one on the right slows the four quadrant vessels in the tank, with one already moved into final location.

As a feasibility study, a mock side vessel was slung under the Yates cage, taken down the shaft, and transported to the cart-wash area just outside the LUX experimental hall. We have studied the process of installing the acrylic vessels into the LUX/LZ water tank using a detailed computer model. The acrylic vessel will be transported in a horizontal position to the deck immediately above the water tank. The vessel will then be rotated using lifting eyes at the top and bottom. The left-hand drawing in Figure 4.4.2 demonstrates one step of this process, near the point that requires maximum clearance above the deck. The vessel is lowered in vertical position into the water tank and then transported radially outward to near the wall of the tank.

The right-hand drawing in Figure 4.4.2 shows the assembly step at which all of the quadrant vessels are in the tank, and the first one is being brought into place around the cryostat. A white diffuse reflector, Tyvek, is strapped with the foam around the cryostat.

The vessels will be fabricated by Reynolds Polymer Technology of Grand Junction, Colorado. Fabrication will take place during calendar 2017.

### 4.4.2 PMT Supports

The LAB scintillation light is viewed by 120 8 inch PMTs in a cylindrical array of 20 ladders with six PMTs each. Figure 4.4.3 shows the plan view of the PMT support system. The PMT faces are positioned 84 cm from the outer-detector tank wall. The water between the PMTs and the scintillator vessel shields the active detector elements from radioactivity in the PMT assemblies. In this location, the PMTs also see the Cherenkov light from cosmic-ray muons passing through the water.

The PMT ladders are attached to the top and bottom of the water tank, at a radius of 282 cm. The PMT frame has been adapted from from the Daya Bay desin. A FINEMET magnetic shield to isolate the performance from the local magnetic field can be deployed The PMT cables run directly from the PMTs through

one of the ports in the top of the water tank to an electronics rack outside. Strain relief is applied at the port and on the ladders.

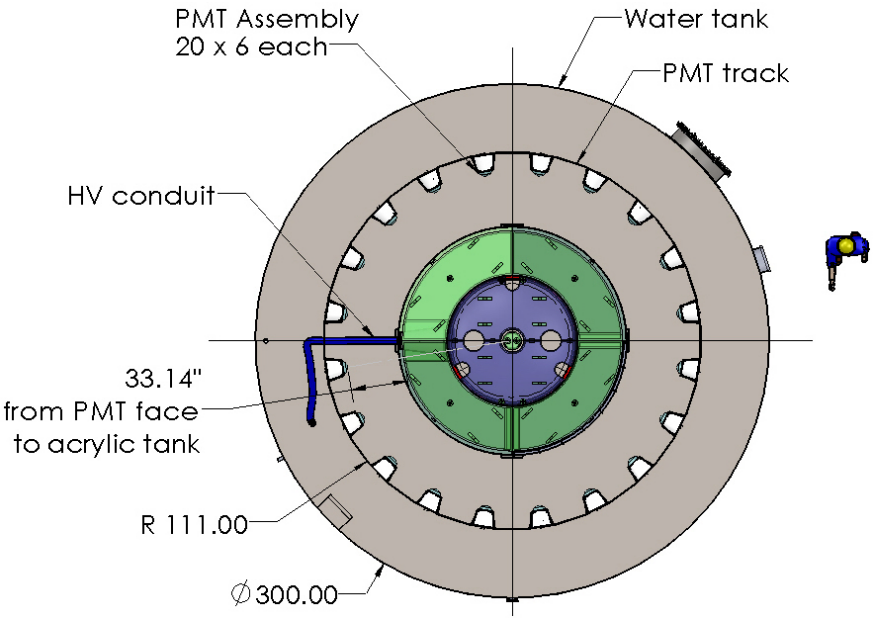


**Figure 4.4.3:** Plan view of the PMT support system. The 20 PMT ladders are mounted to a circular track on the roof of the water tank.

An optical calibration system (OCS) will be deployed on the support structure, and consists of 35 duplex optical fibers driven by LEDs. This system will enable monitoring of the response of the PMT system, and is described in Section 4.7.

### 4.4.3 Scintillator Distribution System

Each of the scintillator vessels has one input and one output line. The lines are Teflon® tubing, with strain relief to the PMT ladders. All lines terminate at a feedthrough panel in the 2 foot flange on the north side of the lid to the water tank. To reduce pressure on the acrylic tanks, a 100 gallon reservoir will be suspended from the floor beams above and next to the north flange of the water tank.

The Gd-LS will be taken underground in 55 gallon drums. Secondary containment will be provided for all of the lines carrying scintillator. All volumes to be filled with Gd-LS will first be purged with dry nitrogen, and all unfilled gas volumes will be kept purged with dry nitrogen to reduce contamination from atmospheric $^{85}$Kr.

To reduce the differential pressure inside and outside the vessels, they will be co-filled with the water tank that encloses them. The hydrostatic pressure on the outer surface of the side vessels varies during the filling process from 1 psi to 7.8 psi, while the pressure on the inside from the scintillator varies from 1.7 psi to 7.6 psi. The 100 gallon reservoir is connected to each vessel and filled to match the internal pressure to the outside pressure.

## 4.5 Liquid Scintillator

We chose Gd-LS for the detection medium to achieve excellent efficiency for neutrons and gammas that reach the outer detector. Various organic liquid scintillators have been used for neutron tagging due to their

production of relatively large numbers of photons at low energies of a few MeV. The neutron-capture reaction occurs on the hydrogen in the organic scintillator, $n + p \rightarrow d + \gamma$, but the cross section is only 0.33 b, with a neutron-capture time of about 200 µs. The single 2.2 MeV $\gamma$ is also in the energy range of natural radioactivity.

Gadolinium-loaded scintillators have been used in several experiments designed to detect neutrons produced by inverse beta decay from reactor antineutrinos. There are several compelling advantages of adding Gd to the liquid scintillator (LS):

- The (n,$\gamma$) cross section for natural Gd is very high, 49 kb, with major contributions from $^{155}$Gd and $^{157}$Gd isotopes. Because of this high cross section, only a small concentration of Gd, 0.1 % by mass, is needed to dominate over neutron capture on protons.
- The neutron-capture reaction on Gd releases 8 MeV of energy in a cascade of 3–4 $\gamma$ rays. The efficiency for detecting at least one of these gammas is very high.
- The time delay for the neutron capture is also significantly shortened to 30 µs in scintillator doped with 0.1 % Gd, compared to a time of 200 µs in undoped scintillator. This means the veto window can be reduced by a factor of 7, reducing the deadtime of the outer detector by the same factor.

To detect the low-neutron/gamma backgrounds with high efficiency, the Gd-LS must have the following key properties:

1. Long optical attenuation length, >10 m at 430 nm;
2. High light yield, 9,000 /MeV;
3. Ultralow impurity content, mainly of the natural radioactive contaminants, such as U, Th, and K; and
4. Long-term chemical stability, over the lifetime of the experiment.

All of these properties have been nearly achieved on a large scale for the Daya Bay experiment. We are adopting the same formulation and fabrication techniques to take advantage of this proven performance

It is necessary to avoid any chemical decomposition, hydrolysis, formation of colloids, or polymerization, which over time can lead to development of color, cloudy suspensions, or formation of gels or precipitates in the scintillator, all of which can degrade the scintillator. Recent successful demonstration of the above-mentioned key items has been done by reactor electron antineutrino experiments using LAB-based, 0.1 % Gd-loaded scintillator.

Assessments of the U/Th contaminations in the Daya Bay scintillator show that Daya Bay has already achieved levels nearly acceptable for the LZ experiment. The LZ goal is based upon limiting rate from gamma rays, betas, and alphas in the LXe fiducial volume to a rate lower by a factor of 8 than that expected from other sources, to achieve deadtime below 5 percent. The dominant source of rate in the OD system is the leakage of gamma rays from the walls of the SURF cavern through the top and bottom of the water shield, and will contribute of order 100 Hz to the OD rates.

The U/Th contamination goals for the scintillator are <1.3 ppt and <4.5 ppt by mass, respectively. Four of the five scintillator ingredients–$GdCl_3$ , LAB, PPO, and bis-MSB–of the scintillator mixture have already been analyzed for U/Th contamination by LZ, and met the goals for Gd-LS. Since the measurements exceeded the original goals, we have changed the goals to be equal to the measurements where measurements have been performed.

These goals for each component are summarized in Table 4.5.1. The goal for $^{238}$U is a factor of 15 below the level achieved by the Daya Bay collaboration. In addition, a level of 0.8 ppt of $^{40}$K is the required, which is a factor of 9 lower than achieved by Daya Bay. KAMLAND and Borexino reached contamination levels

orders of magnitude lower by filtering and stripping the scintillator solvent. We plan to meet the targets by inserting a second pass of purification into the production process, one step beyond that applied by the Daya Bay collaboration.

The goal for $^{14}$C is aggressive, and to meet it, underground sources must be used for all organics. Should the $^{14}$C level be higher than expected, the scintillator threshold will be raised from 100 keV$_{ee}$ to above the $^{14}$C endpoint of 156 keV$_{ee}$. The scintillator must be kept out of contact with the atmosphere to avoid $^{85}$Kr, and the levels of $^{85}$Kr observed in both KAMLAND and Borexino would contribute a negligible rate to LZ.

**Table 4.5.1:** Radioactive impurities in LAB-based Gd-LS. The left side contamination goals for various components of the Gd-LS. Cells shaded yellow are based on screening measurements. Propagation of these contributions to the proposed Gd-LS mixture is summarized in the last four columns. The goals (requirements) keep the rate contribution to the OD below 15 Hz (80 Hz) from these sources.

| | Raw values (ppt) | | | | Gms/liter | Values in 0.1% Gd-LS (ppt) | | | |
|---|---|---|---|---|---|---|---|---|---|
| Item | $^{238}$U | $^{232}$Th | $^{40}$K | $^{14}$C | in Gd-LS | $^{238}$U | $^{232}$Th | $^{40}$K | $^{14}$C |
| LAB | 0.004 | 0.007 | 0.5 | $12\times10^{-6}$ | 860 | 0.004 | 0.007 | 0.5 | $12\times10^{-6}$ |
| Gd | 100 | 100 | 52 | | 0.86 | 0.17 | 0.17 | 0.09 | |
| PPO | 150 | 640 | 27 | $110\times10^{-6}$ | 3 | 0.5 | 2.2 | 0.09 | $0.37\times10^{-6}$ |
| TMHA | 180 | 650 | 27 | $140\times10^{-6}$ | 3 | 0.6 | 2.1 | 0.09 | $0.44\times10^{-6}$ |
| bis-MSB | 210 | 190 | 50 | $19\times10^{-3}$ | 0.015 | 0.004 | 0.003 | 0.001 | $0.32\times10^{-6}$ |
| **Total** | | | | | 867.2 | **1.3** | **4.5** | **0.8** | $\mathbf{13\times10^{-6}}$ |
| **Requirement** | | | | | | **10** | **20** | **3** | $\mathbf{15\times10^{-6}}$ |
| **Daya Bay** | | | | | | **20** | **4** | **7** | |

The production of the Gd-LS is being led by the Brookhaven National Laboratory (BNL) group. The manager of the LS production effort has considerable relevant experience, including supervision of the development and production of the same scintillator for the Daya Bay experiment. The development of LZ scintillator will be undertaken in two phases: a demonstration phase (to reach ppt levels), followed by a production phase for deployment. The BNL group has a state-of-the-art Liquid Scintillator Development Facility equipped with a variety of instruments (e.g., UV, IR, XRF, LC-MS, medium-scale mixing reactor, thin-film distillatory, 2 m attenuation length system, etc.) for quality assurance that are essential to quality control of the scintillator.

To test whether Gd-LS from the demonstration phase meets all the goals in Table 4.5.1, we have built a "LS screener," consisting of an acrylic vessel that can hold about 24 kg of Gd-LS viewed by three very low-background PMTs. We deploy the LS screener in the LZ water tank in November, 2016 through January 2017.

The most cost-effective plan for the 17.2 t of LZ low-background Gd-LS production is to carry out the production at the BNL facility and ship the synthesized scintillator to SURF for filling. The scintillator will be produced at a rate of 0.5 t per week and will be stored in 55-gallon PTFE-lined drums, which are then shipped to SURF for storage. The purification methods for all components of the Gd-doped scintillator are developed and will be applied to each component before synthesis.

## 4.6 Light Detection

### 4.6.1 Photomultipliers

Building on the successful use of the Hamamatsu R5912 PMTs in experiments such as MILAGRO, AMANDA, and most recently Daya Bay, the LZ outer detector will use 120 of these same PMTs. The two existing models for this PMT are R5912 and R5912-02. The latter possesses four more dynode stages and provides higher gain, at the cost of higher dark current and slightly degraded timing characteristics. As LZ does not need the additional gain, the less-expensive model R5912 was chosen. Even for this model, several subcategories exist that represent various quality levels of glass window and photocathode materials. Our assessment of radioactivity levels concluded that the basic model was sufficient for LZ needs and requirements.

**Table 4.6.1:** Characteristics of the R5912 PMTs, from the Hamamatsu data sheets.

| Characteristic | Value |
|---|---|
| Number of dynode stages | 10 |
| Window material | Borosilicate glass |
| Photocathode material | Bialkali |
| Minimum photocathode effective area | 284 $cm^2$ |
| Typical bias voltage for gain of $1 \times 10^7$ | 1,500 V |
| Maximum voltage | 2,000 V |
| Mean QE at 390 nm | 25 % |
| Pressure rating | 0.7 MPa |
| Radioactivity levels per PMT (all components) | $^{238}$U: 1,200 mBq<br>$^{232}$Th: 680 mBq<br>$^{40}$K: 920 mBq |

The R5912 PMTs are suitable for the outer detector for the following reasons:

1. The spectral response ranges from 300 nm to 650 nm, with a peak wavelength at 420 nm. This matches well the scintillation light from the LAB mix between 390 nm to 440 nm. The quantum efficiency also covers the relevant range, with an average expected value of ~25 % at 430 nm.

2. The PMTs will be submerged in up to 6 m water and must be able to operate in this environment. Daya Bay has been able to demonstrate successful operation of the R5912 assembly at higher pressures than those required for LZ. This experiment used the same assembly that LZ will use.

3. The radioactivity levels of the PMTs and assembly are a fairly weak constraint, thanks to the minimum 84 cm of water that separate them from any active detector volume. The water buffer typically reduces the integrated flux of incoming gammas by more than 2 orders of magnitude, before taking into account geometric effects. For the event rate in the Xe target, the 80 cm of water plus the thickness of the scintillator make the R5912 contribution largely subdominant to internal sources, for both gammas and neutrons. In the scintillator itself, the simulated event rate from PMT radioactivity is <4 Hz (<4 % deadtime would be caused by 100 Hz).

The R5912 PMTs and waterproof assemblies will undergo rigorous individual testing to fully characterize the response and to validate uniform operation and long-term stability for the lifetime of the detector. These tests will include individual electrical behavior, gain measurements, linearity, after-pulsing, dark current, and dark count. In addition, the PMTs will be radioactively screened to make sure the activities are consistent with the values listed in Table 4.6.1.

## 4.7 Optical Calibration System

An optical calibration system (OCS) will be used to monitor the performance of the outer detector and to maintain calibration. The light will be emitted from 30 LED-driven duplex optical fibers mounted on the PMT support system walls, and 5 duplex fibers routed underneath the bottom tanks. The system on the PMT walls will monitor overall system response, including attenuation in the Gd-LS and in the water. Some fibers under the bottom tanks will use light wavelengths tuned to monitor acrylic transmission.

The OCS will enable the monitoring of the response of the OD system at the level of 3 percent, in time and in space. Systems will monitor the stability of the OCS light sources and supporting light detectors. The range of light outputs covered by the OCS focus on the threshold of $\approx$100 $\mathrm{keV_{ee}}$ up to the expectation of the largest signals from a neutron capture on gadolinium, about 10 $\mathrm{MeV_{ee}}$. The OCS will also enable the monitoring and calibration of large signals from penetrating muons.

## 4.8 Threshold, singles rate, deadtime

As described above, a neutron capture in the Gd-LS releases either a few gammas of total energy 8 MeV or a single gamma of energy 2.2 MeV. The neutron-detection efficiency is therefore quite high with the 100 $\mathrm{keV_{ee}}$ threshold planned for the outer detector, which corresponds to about 13 photoelectrons observed. Figure 4.8.1 shows the simulated inefficiency for vetoing 1 MeV background neutrons that scatter once in the LXe TPC as a function of threshold in $\mathrm{keV_{ee}}$. These simulations indicate that the efficiency of the combined veto for neutrons escaping the LXe TPC is about 97 %.

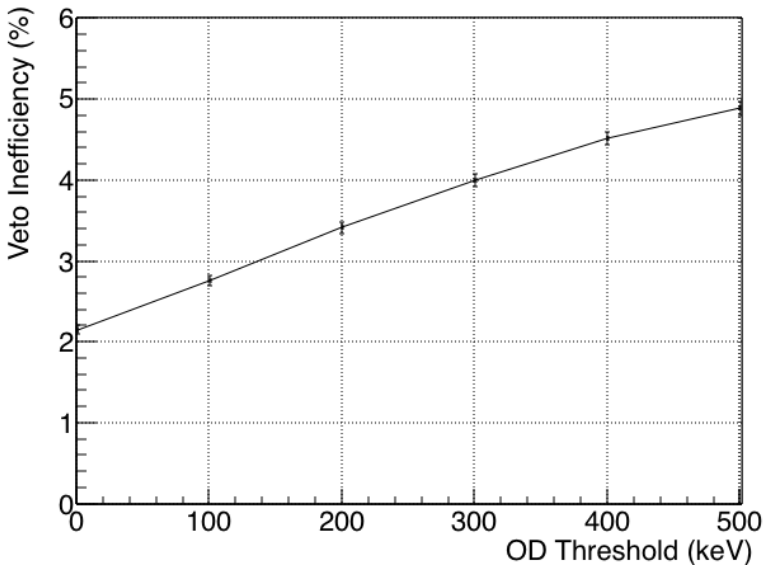


**Figure 4.8.1:** Inefficiency for vetoing neutrons from fixed contamination in detector components that scatter once in the xenon TPC, plotted as a function of threshold in the OD. For this simulation, the skin veto threshold is taken to be 100 keV.

We will read out the outer-detector PMTs each time the LXe TPC produces a trigger, without need of a hardware threshold. We will therefore be able to apply the veto offline, with parameters carefully selected to optimize the veto efficiency. Our goal is to apply neutron veto over a time window of 500 µs with a threshold of 100 $\mathrm{keV_{ee}}$. In

addition, we will apply a gamma veto over a much tighter time window of 1 µs with a threshold of 100 $keV_{ee}$. There will be an outer-detector hardware trigger to calibrate and monitor the background environment.

The sensitivity of the outer detector is estimated to be about 130 photoelectrons/MeV from simulation of LZ and this agrees with benchmarks against similar detectors. Thus, a 100 $keV_{ee}$ threshold corresponds to about 13 photoelectrons, and the trigger rate will be dominated by alphas, gammas, and betas from the U and Th chains.

Because the time of the low-energy scatter in Xe is determined well by measuring the prompt S1 light, the neutron veto window will be determined by the capture time for neutrons. Our goal is a 500 µs veto window. Our formal requirement is on deadtime, of <5 %. This requirement can be met with a variety of combinations of thresholds and veto windows. Our goal is to keep the rate in the outer detector below 100 Hz, and use a veto window of 500 µs, but currently our simulations show that we could achieve our deadtime and ineffiency requirements with an outer detector rate as high as 300 Hz and a veto window of 170 µs. The radiopurity goals in Table 4.5.1 keep the overall background rate in the OD below 100 Hz.

Ultimately, the of the veto window and threshold needed for high-efficiency neutron tagging will be determined by studying it with calibration data.

## 4.9 Environment, Safety, and Health Considerations

The most important safety issue to consider underground is flammability. The flashpoint for LAB is 120 °C to 140 °C, which makes it a Class IIIB liquid, the lowest hazard category. A Class IIIB liquid is a combustible liquid with a flashpoint at or above 200 °C (93 °C). OSHA flammable and combustible liquid regulations do not apply to IIIB liquids. The boiling point is greater than 250 °C and the melting point is below −70 °C, so it is very stable as a liquid. The density of LAB is 0.86 $gm/cm^3$, significantly less than water. In addition, it has very low solubility in water.

The primary risk to consider is a crack in one of the acrylic vessels. The first preventive step is to thoroughly check the integrity of the vessel before introducing the scintillator liquid into it. The second is to monitor the vessel carefully during the filling process. The water tank serves as a secondary containment system for the scintillator. We will also be able to separate LAB from the water in the water treatment. If a significant leak is observed, we will skim the surface of the water to recover most of the scintillator, and then remove the residual scintillator by distillation.

## 4.10 Bibliography

[1] M. Apollonio *et al.* (CHOOZ), Eur. Phys. J. **C27**, 331 (2003), arXiv:hep-ex/0301017 [hep-ex].

[2] F. Boehm *et al.*, Phys. Rev. Lett. **84**, 3764 (2000), arXiv:hep-ex/9912050 [hep-ex]; A. G. Piepke, S. W. Moser, and V. M. Novikov, Nucl. Instrum. Meth. **A432**, 392 (1999), arXiv:nucl-ex/9904002 [nucl-ex].

[3] F. P. An *et al.* (Daya Bay), Nucl. Instrum. Meth. **A685**, 78 (2012), arXiv:1202.6181 [physics.ins-det]; X. Guo *et al.* (Daya Bay), "A Precision measurement of the neutrino mixing angle $\theta_{13}$ using reactor antineutrinos at Daya-Bay," (2007), proposal, arXiv:hep-ex/0701029 [hep-ex].